A Generalized Multiple Discrete Interaction Approximation for resonant four-wave interactions in wind wave models ☆

Hendrik L. Tolman *

NOAA/NCEP/EMC, Marine Modeling and Analysis Branch, 5830 University Research Court, College Park, MD 20740, USA

ABSTRACT

For several decades, the Discrete Interaction Approximation (DIA) for nonlinear resonant four-wave interactions has been the engine of third-generation wind-wave models. The present study presents a Generalized Multiple DIA (GMD) which expands upon the DIA by (i) expanding the definition of the representative quadruplet, (ii) formulating the DIA for arbitrary water depths, (iii) providing complimentary deep and shallow water scaling terms and (iv) allowing for multiple representative quadruplets. The GMD is rigorously derived to be an extension of the DIA, and is backward compatible with it. The free parameters of the GMD are optimized holistically, by optimizing full model behavior in the WAVEWATCH III® wave model as reported in a companion paper. Here, a cascade of GMD configurations with increasing complexity, accuracy and cost is presented. First, the performance of these configurations is discussed using idealized test cases used to optimize the GMD. It is shown that in deep water, GMD configurations can be found which remove most of the errors of the DIA. The GMD is also capable of representing four-wave interactions in extremely shallow water, although some remaining spurious behavior makes applications of this part of the GMD less suitable for operational wave models. Finally, several GMD configurations are applied to an idealized hurricane case, showing that results from idealized test cases indeed are representative for real-world applications, and confirming that such GMD configurations are economically feasible in operational wind wave models. Finally, the DIA results in surprisingly large model errors in hurricane conditions.

Published by Elsevier Ltd.

1. Introduction

Numerical modeling of wind waves has been a subject of interest for many decades, arguably starting in earnest with operational wave prediction for the D-day invasion of Normandy in 1944 (Sverdrup and Munk, 1947). Initial models considered representative wave heights and periods only. Starting with Gelci et al. (1956, 1957), wind wave modeling has focused on spectral descriptions of the wave field based on earlier work with radio waves of Rice (1944). Most such wave models are based on some form of the spectral balance equation of Hasselmann (1960).

$$\frac{DF}{Dt} = S_{tot} = S_{in} + S_{nl} + S_{ds}, \tag{1}$$

where F is the variance or energy spectrum of the wind waves, and S represent sources and sinks. Many models now use a balance equation for the wave action spectrum to account for (linear) wave–current interactions, based on the work of Bretherthon and Garrett

(1968). Otherwise, the latter equation retains all relevant characteristics of Hasselmann's equation (1).

The left hand side of Eq. (1) represents linear wave propagation. The right side of Eq. (1) represents the total effects of sources and sinks (S_{tot}) on spectral energy. Traditionally, the sources and sinks essential for describing wave growth and decay are divided into wind input (S_{in}), nonlinear interactions (S_{nl}) and dissipation (S_{ds}).

In these source terms, the four-wave resonant nonlinear interactions play an important role. All other source terms are operating locally in spectral space, increasing or decreasing the local energy or action density. Hence, they can only make individual wave components higher or lower. Nonlinear interactions redistribute energy over spectral space, and it is generally believed that this fourth-order nonlinear process is the lowest order process (in deep water) able to redistribute energy over the spectrum. Therefore, it is critical to reproduce the observed down-shifting of energy in frequency space during wave growth. Furthermore, these interactions stabilize the spectral shape at high frequencies. These essential characteristics of the four-wave nonlinear interactions were solidly established in the Joint North Sea Wave Experiment (JONSWAP, Hasselmann et al., 1973). Subsequently, an international wave model intercomparison study (SWAMP group, 1985) concluded that it is essential to explicitly account for these interactions in

wave models. This resulted in the development of the first so-called third-generation wave model (WAM, WAMDIG, 1988). Our understanding of these nonlinear interactions goes back to the 1960s, with seminal papers by Phillips (1960), Hasselmann (1962, 1963a,b) and Zakharov (1968), reviews of the interactions and their impact can be found, for instance, in Masuda (1980), Phillips (1981), Young and Van Vledder (1993), Komen et al. (1994) and Van Vledder (2006).

The nonlinear interactions describe the resonant exchange of energy, momentum and action between a "quadruplet" of four spectral components with wavenumber vectors $\boldsymbol{k}_1$ through $\boldsymbol{k}_4$ and (radian) frequencies σ_1 through σ_4 ($\sigma = 2\pi f$) satisfying the resonance conditions (Hasselmann, 1962, 1963a):

$$\boldsymbol{k}_1 + \boldsymbol{k}_2 = \boldsymbol{k}_3 + \boldsymbol{k}_4, \tag{2}$$

$$\sigma_1 + \sigma_2 = \sigma_3 + \sigma_4, \tag{3}$$

where wavenumber $k = \|\boldsymbol{k}\|$ and frequency σ satisfy the dispersion relation

$$\sigma^2 = gk \tanh kd \tag{4}$$

and where g is the acceleration of gravity and d is the (mean) water depth. The interactions are conventionally expressed in terms of the rate of change of the action spectrum in terms of the wavenumber vector $\boldsymbol{k}$, and are computed using a Boltzmann integral as

$$\frac{\partial n_1}{\partial t} = \int \int \int G(\boldsymbol{k}_1, \boldsymbol{k}_2, \boldsymbol{k}_3, \boldsymbol{k}_4) \, \delta_k \, \delta_\sigma$$
$$\times [n_1 n_3 (n_4 - n_2) + n_2 n_4 (n_3 - n_1)] \, d\boldsymbol{k}_2 \, d\boldsymbol{k}_3 \, d\boldsymbol{k}_4, \tag{5}$$

where n_i is the action density at component i, $n_i = n(\boldsymbol{k}_i)$, G is the coupling coefficient (Webb, 1978; Herterich and Hasselmann, 1980), and δ_k and δ_σ are delta functions representing the resonance conditions (2) and (3). An important feature used in computing nonlinear interactions is the symmetry of computations related to the concept of detailed balance (Hasselmann, 1966; Komen et al., 1994, Section 2.3.8), which states that for quadruplets satisfying the resonance conditions (2) and (3) action changes δn are related as

$$-\delta n_1 = -\delta n_2 = \delta n_3 = \delta n_4. \tag{6}$$

Much progress has been made on the efficient solution of these equations, by, for instance, Masuda (1980), Tracy and Resio (1982), Resio and Perrie (1991), Komatsu and Masuda (1996) and Van Vledder (2000), and a recent review can be found in Van Vledder (2006).

With the above studies, numerical implementations of the full nonlinear interactions according to Eq. (5) are well established. Portable computational packages are available (e.g., Van Vledder, 2002a, 2006), and have been implemented in wave models like SWAN and WAVEWATCH III®. However, even the optimized full interaction routines are computationally expensive due to the multiple integrations over the spectral space and the complexity of the interaction coefficient G. When applied in numerical wave models, these algorithms are orders of magnitude more computationally expensive than all other aspects of the wave model combined. Economical feasibility of wave models at operational forecast centers now allows for interactions to take up most of the computational resources, but requires that they cannot be more than one order of magnitude more expensive that the remainder of the wave model.[1]

The seminal breakthrough making operational third-generation wave models feasible was the development of the Discrete Interaction Approximation (DIA) by Hasselmann et al. (1985), denoted

here as HHAB. HHAB introduced several simplifications to the computation of the nonlinear interactions. (i) The multi-dimensional integral of Eq. (5) is replaced by what HHAB define as a "discrete equivalent" while using the concept of detailed balance from Eq. (6). (ii) The complex interaction coefficient G is replaced by a simple scaling function, which (iii) is considering deep water only. With these assumptions and simplifications Eq. (5) becomes [HHAB Eq. (5.4)]

$$\begin{pmatrix} \delta n_1 \\ \delta n_2 \\ \delta n_3 \\ \delta n_4 \end{pmatrix} = \begin{pmatrix} -1 \\ -1 \\ 1 \\ 1 \end{pmatrix} C B \left[n_1 n_2 (n_3 + n_4) - n_3 n_4 (n_1 + n_2) \right] \Delta \boldsymbol{k} \Delta t, \tag{7}$$

where C is a proportionality constant, B a scaling function and $\Delta \boldsymbol{k}$ and Δt are an infinitesimal phase-space element and time interval, respectively. Furthermore, (iv) only a subset of all resonant quadruplets is used, defined by Eqs. (2) and (3), and by

$$\left. \begin{array}{l} \boldsymbol{k}_1 = \boldsymbol{k}_2 \\ \sigma_3 = (1 + \lambda)\sigma_1 \\ \sigma_4 = (1 - \lambda)\sigma_1 \end{array} \right\}, \tag{8}$$

where λ is a constant. In the initial applications of the DIA in the WAM model (WAMDIG, 1988) $\lambda = 0.25$. This setting is still used in most third-generation models.

Note that the "discrete" interactions (7) computed for a representative quadruplet (8) replace an integration in spectral space along a locus of possible interaction configurations (e.g., Webb, 1978; Tracy and Resio, 1982). This represents a systematic difference between solving the full Boltzmann integration and the discrete approach, that cannot be removed by simply adding representative quadruplets. In this sense the "discrete equivalent" introduced by HHAB is not fully "equivalent" with the exact interactions.

For these quadruplets, the corresponding discrete source term contributions $\delta S_{nl}(f, \theta)$ for the energy spectrum $F(f, \theta)$ are given as

$$\begin{pmatrix} \delta S_{nl,1} \\ \delta S_{nl,3} \\ \delta S_{nl,4} \end{pmatrix} = D \begin{pmatrix} -2 \\ 1 \\ 1 \end{pmatrix} C g^{-4} f_1^{11} \times \left[F_1^2 \left(\frac{F_3}{(1+\lambda)^4} + \frac{F_4}{(1-\lambda)^4} \right) - \frac{2 F_1 F_3 F_4}{(1-\lambda^2)^4} \right], \tag{9}$$

where f and θ are the spectral frequency and direction, respectively, $F_i = F(f_i, \theta_i)$, $\delta S_{nl,1} = \delta S_{nl}(f_i, \theta_i)$, and C is the proportionality constant, determined by model tuning ($C = 3 \times 10^7$ in WAM, $C = 1 \times 10^7$ in WAVEWATCH III). Finally, D is a scaling function to account for effects of limited water depths (Hasselmann and Hasselmann, 1985), first introduced in the WAM model (WAMDIG, 1988), and uniformly applied to the entire source term

$$D = 1 + \frac{5.5}{\bar{k}d} \left[1 - \frac{5}{6} \bar{k}d \right] e^{-1.25 \bar{k}d}. \tag{10}$$

Here $\bar{k}d$ is the mean relative water depth. Note that in this shallow water approach, resonance conditions and interaction contributions are still evaluated assuming deep water. Note also that Eq. (9) explicitly assumes a logarithmic discrete frequency distribution

$$\sigma_{i+1} = X_\sigma \sigma_i, \tag{11}$$

where i is the discrete frequency counter and X_σ is the frequency increment factor. In the original WAM model application $X_\sigma = 1.1$.

With its simplifications the DIA defined by Eqs. (8)–(10) becomes comparable in terms of computational costs with the rest of a typical wave model. In a model with advanced (expensive) numerics like WAVEWATCH III, the DIA accounts for roughly 25% of the computational costs of the model.

---

[1] Based on practical experience at NCEP.

Whereas the DIA was essential for the development of third-generation wave models, it also has been recognized to have serious shortcomings. HHAB recognized that the DIA gives a realistic representation of the exact interactions for the low-frequency positive lobe only, and that it results in spectra with a directional spread that is too broad. It is therefore not surprising that much effort has been put into finding alternative accurate yet economical parameterizations for the nonlinear interactions (e.g., Van Vledder et al., 2000). Many of such approaches attempt to trade speed for accuracy, either by reducing the computations for the exact interactions, or by adding more complexity to the DIA. The former approach is typically characterized by applying various filtering techniques to the nonlinear interactions (e.g., Snyder et al., 1998; Hashimoto et al., 2002). The latter approach allows for more complex descriptions of the representative quadruplet, addition of more representative quadruplets, and additional tuning parameters in the basic scaling function (e.g., Ueno and Ishizaka, 1997; Hashimoto and Kawaguchi, 2001; Van Vledder, 2001, 2002b). A 'midpoint' between these approaches appears to be the SRIAM algorithm (e.g., Komatsu, 1996; Tamura et al., 2008). Unfortunately, this approach is not yet fully published in English literature.

The present study focuses on expanding the DIA to improve its accuracy while remaining sufficiently economical for use in operational wave models. This study has explored all previously suggested expansions of the DIA, and full shallow water scaling capabilities are added. The resulting Generalized Multiple DIA (GMD) is presented in Section 2, and its numerical implementation is discussed in Section 3. The ongoing development of the GMD has been documented in full detail in various reports, conference proceedings and papers (Tolman, 2003, 2004, 2005, 2008b, 2009a, 2010; Tolman and Krasnopolsky, 2004).

An integral part of developing a GMD is the optimization of the free parameters in the approximation. Traditionally, this has been done by computing exact interactions for test spectra, and subsequently fitting approximations to most accurately represent the exact interactions. However, due to the highly nonlinear nature of the interactions, this is no guarantee for good overall model behavior (e.g., Tolman, 2004). With this in mind, a holistic optimization approach has been introduced in Tolman (2005) and Tolman and Krasnopolsky (2004). In this approach, the overall model integration behavior is considered for several idealized test cases to optimize free parameters in the GMD. Details of the optimization procedures are presented in a companion paper (Tolman and Grumbine, 2013), and its results are presented in Section 4. Test results for the GMD for practical applications are presented in Section 5. A discussion and conclusions are presented in Sections 6 and 7, respectively.

The holistic optimization approach requires a full wave model. Here the WAVEWATCH III model is used (Tolman, 2009b, henceforth denoted as WW3), using its default settings with the exception of nonlinear interaction approaches. The DIA and the exact interaction approaches are available in the standard model, whereas the GMD has been added.

2. The Generalized Multiple Discrete Interaction Approximation

In the present study, the same starting point (7) is used as in HHAB. Unlike in HHAB, the Generalized Multiple DIA (GMD) will be constructed for arbitrary water depths. First, definitions of the representative quadruplet are considered in Section 2.1. Spectral definitions and conservation properties of the GMD are considered in Sections 2.2 and 2.3. Scaling considerations are discussed in Section 2.4, and the final GMD formulations are presented in Section 2.5.

Note that this approach to construct a more general DIA has been taken before by Rasmussen (1998), Van Vledder (2002b) and Van Vledder and Bottema (2002). The present study expands upon the former studies, particularly with respect to the definition of the representative quadruplet, the assessment of the impact of the choice of various spectral descriptions, and the construction of scaling functions.

2.1. Representative quadruplets

The representative quadruplet is defined by the resonance conditions (2) and (3) and by some additional restrictions like Eq. (8). The latter equation defines the representative quadruplet by a single parameter (λ). Van Vledder (2001) has shown that a minimum of three parameters is required to produce arbitrary representative quadruplets.

For the GMD the following general quadruplet layout is used,

$$\left.\begin{array}{l} \sigma_1 = a_1\,\sigma_r \\[4pt] \sigma_2 = a_2\,\sigma_r \\[4pt] \sigma_3 = a_3\,\sigma_r \\[4pt] \sigma_4 = a_4\,\sigma_r \\[4pt] \theta_2 = \theta_1 \pm \theta_{12} \end{array}\right\}, \tag{12}$$

where $a_1 + a_2 = a_3 + a_4$ to satisfy the resonance condition (3), σ_r is a reference frequency, and θ_{12} is the angular gap between the wavenumbers $\boldsymbol{k}_1$ and $\boldsymbol{k}_2$. The latter parameter can either be implicit to the quadruplet definition, or can be an explicitly tunable parameter.

A one, two, and three-parameter quadruplet definitions as used in this study are defined in Table 1. The one-parameter (λ) quadruplet layout represents the traditional DIA approach. The two-parameter (λ, μ) quadruplet layout is taken from Tolman (2004). In this approach, $\boldsymbol{k}_1$ and $\boldsymbol{k}_2$ are modified in the same ways as $\boldsymbol{k}_3$ and $\boldsymbol{k}_4$ in the traditional DIA approach, and θ_{12} is implied by the choice of μ. The three-parameter ($\lambda, \mu, \theta_{12}$) quadruplet layout is an extension of the two-parameter layout with θ_{12} as an additional free parameter. The latter quadruplet definition can be considered as the symmetric and compact equivalent to the three-parameter quadruplet definition introduced by Van Vledder (2001) (see Tolman, 2005, Section 5.1). Since the discrete contributions to the interactions are computed for each discrete spectral grid point, the relation between the quadruplet and the discrete spectral grid points (σ_d, θ_d) is also outlined in the table, with the discrete direction θ_d always aligned with the direction of $\boldsymbol{k}_1 + \boldsymbol{k}_2$.

In Section 2.1 of Tolman (2008b) valid layouts of quadruplets as a function of their free parameters are analyzed in detail. For deep water and the one- and two-parameter quadruplet definition valid quadruplets are found for

$$0 \leqslant \mu < \lambda \leqslant 0.5, \tag{13}$$

which for the three-parameter quadruplet definition expands to

Table 1
One, two, or three parameter definitions of the representative quadruplet in the GMD. $\boldsymbol{k}_d$ or (σ_d, θ_d) represents the discrete spectral grid point for which the discrete interaction contributions are evaluated. All quadruplets are aligned with the discrete directions by taking $\boldsymbol{k}_1 + \boldsymbol{k}_2 /\!/ \boldsymbol{k}_d$.

Parameters	a_1	a_2	a_3	a_4	θ_{12}	σ_r
(λ)	1	1	$1+\lambda$	$1-\lambda$	0	σ_d
(λ, μ)	$1+\mu$	$1-\mu$	$1+\lambda$	$1-\lambda$	Implied[a]	σ_d
($\lambda, \mu, \theta_{12}$)	$1+\mu$	$1-\mu$	$1+\lambda$	$1-\lambda$	Free	$\frac{\sigma_d}{1+\mu}$

[a] Assuming $\boldsymbol{k}_1 + \boldsymbol{k}_2 = \boldsymbol{k}_3 + \boldsymbol{k}_4 = 2\boldsymbol{k}_d$.

$$\left.\begin{array}{l} 0 \leqslant \mu < \lambda \leqslant 0.5 \\ 0 \leqslant \theta_{12} \leqslant 180° \\ \lambda \text{ valid for } (\mu, \theta_{12}) \text{ for } kd \to \infty \end{array}\right\}. \tag{14}$$

Furthermore, it is shown that such quadruplets are valid for arbitrary depths, although this does not include all valid quadruplets in shallow water.

2.2. Spectral description

Eq. (7) from which the DIA is expressed in terms of the action spectrum $n(\mathbf{k})$, whereas the final DIA Eq. (9) is expressed in term of the energy density spectrum $F(f, \theta)$. The GMD is derived in terms of the latter spectrum, as this proved to be most conducive to optimization (see Tolman, 2009a).

The transition from the $n(\mathbf{k})$ spectrum to the $F(f, \theta)$ spectrum using the definition of action and conventional Jacobian transformations impacts Eq. (7) in two ways; it impacts the product term in square brackets (henceforth denoted as P_{1234}), and the phase space element Δk. Using the spectral definitions and conventional Jacobian transformations, the spectra are related as

$$n(\mathbf{k}) = \frac{c_g F(f, \theta)}{2\pi k \sigma} \tag{15}$$

and the product term becomes

$$P_{1234} = \frac{1}{(2\pi)^3} \left[\frac{c_{g,1}F_1}{k_1\sigma_1} \frac{c_{g,2}F_2}{k_2\sigma_2} \left(\frac{c_{g,3}F_3}{k_3\sigma_3} + \frac{c_{g,4}F_4}{k_4\sigma_4} \right) \right. $$
$$\left. - \frac{c_{g,3}F_3}{k_3\sigma_3} \frac{c_{g,4}F_4}{k_4\sigma_4} \left(\frac{c_{g,1}F_1}{k_1\sigma_1} + \frac{c_{g,2}F_2}{k_2\sigma_2} \right) \right] \tag{16}$$

Following the arguments and derivation of HHAB, albeit with the full shallow water Jacobians for conversions of spectral densities and spectral phase space elements, the source term contribution $\delta S_{nl,i}$ becomes[2]

$$\delta S_{nl,i} = \frac{\delta n_i}{\Delta \mathbf{k}_i \Delta t} = \mp \frac{2\pi k \sigma}{c_g} \frac{a_i \Delta f}{\Delta f_i} \times \cdots, \tag{17}$$

where the ellipsis represents the constant, scaling function and product terms in Eq. (7). Finally, following HHAB to imply from the logarithmic discrete frequency grid (11) that $a_i\Delta f = \Delta f_i$ (independent of the choice of X_σ), this becomes

$$\begin{pmatrix} \delta S_{nl,1} \\ \delta S_{nl,2} \\ \delta S_{nl,3} \\ \delta S_{nl,4} \end{pmatrix} = \begin{pmatrix} -1 \\ -1 \\ 1 \\ 1 \end{pmatrix} \frac{2\pi k \sigma}{c_g} \times \cdots \tag{18}$$

2.3. Conservation properties

A key property of the nonlinear interactions is the conservation of energy, action and momentum. In the full interactions, defined by Eqs. (2)–(5), the conservation of these three quantities is contained in the quadruplet satisfying the resonance conditions, and in the concept of detailed balance of Eq. (6) (e.g., Webb, 1978). Retaining the resonance conditions and detailed balance in the generic DIA of Eq. (7) assures conservation properties are retained. Webb's observations furthermore imply that details of the computation of the product term P_{1234} and scaling function B or $C'B$ have no impact on conservation properties of the parameterization, and that separate weights can be added to individual terms in P_{1234} (e.g., Ueno and Ishizaka, 1997; Hashimoto and Kawaguchi, 2001; Tolman, 2004) without impacting conservation properties.[3]

A complication in a numerical wave model is that the spectral phase space is discretized, and that discrete phase space elements generally do not coincide with the four components of a (realization of a) quadruplet. Spectral energy densities F_i can only be obtained by interpolation from the discrete phase space

$$F_i = \sum_{j=1}^{4} w_{i,j} F_j, \tag{19}$$

where j represents the four surrounding discrete points in phase space, and where $w_{i,j}$ are the corresponding weight factors. Considering Webb's observations, this interpolation has no impact on conservation properties. Discrete contributions $\delta S_{nl,i}$ to the source term are evaluated at the quadruplet components, and generally need to be distributed over four surrounding points in the discrete phase space. In the traditional DIA this is achieved consistent with the above interpolation as

$$\delta S_{nl,i,j} = w_{i,j} \delta S_{nl,i}. \tag{20}$$

When this distribution of individual interaction contributions is applied to the logarithmic frequency grid (11), it can be shown that wave energy is conserved, and that conservation of action and energy requires that the respective resonance conditions (3) and (2) are satisfied (see Tolman, 2008b, Section 2.2). Consequently, the traditional DIA conserves all properties in deep water, but does not conserve momentum in shallow water, and the latter deficiency is removed in the GMD by evaluating the quadruplet for the actual water depth.

2.4. Scaling considerations

The final building block of a GMD is the scaling function B. In HHAB, no details are given on how this function is derived, but it appears to be based on straightforward dimensional considerations. Here, a more systematic derivation has been performed, following previous work by Van Vledder (2002b). A detailed derivation can be found in Tolman (2008b), Section 2.5. Here only basic concepts and final results will be presented.

The scaling function B in Eq. (7) consists of two main contributions; a scaling function representing the complex interaction coefficient G in Eq. (5), and Jacobians resulting from the transition from Eqs. (5)–(7). Also included in the scaling function are common factors arising in Eqs. (16) and (18), and purely aesthetic factors assuring (i) full backward compatibility from the GMD to the DIA, and (ii) to assure that a degenerate GMD with multiple copies of a single representative quadruplet give the same results as a GMD with a single copy of that quadruplet.

A complication occurs because the factor G describes both 'weak' interactions in deep water and intermediate depths, and 'strong' interactions in extremely shallow water. Whereas the former interactions are described in the traditional DIA, the latter are not. In Section 2.5 of Tolman (2008b), it is shown that complimentary 'deep' and 'shallow' scaling functions can be defined representing the weak and strong interactions, respectively, both with their own proportionality constant C. hence, the product CB in Eq. (7) becomes

$$CB = \frac{1}{n_{q,d}} C_{\text{deep}} B_{\text{deep}} + \frac{1}{n_{q,s}} C_{\text{shal}} B_{\text{shal}}, \tag{21}$$

where C_{deep} and C_{shal} are the proportionality constants, and $n_{q,d}$ and $n_{q,s}$ are the number of representative quadruplets with deep (weak) and shallow (strong) scaling, respectively. Scaling with $n_{q,d}$ and $n_{q,s}$ is added for the above mentioned aesthetic reasons. The 'deep' scaling function is given as

---

[2] See Tolman (2008b), Section 2.4.
[3] Separate tunable constants not considered here, see Tolman (2004).

$$B_{\text{deep}} = \frac{k^{4+m}\sigma^{13-2m}}{(2\pi)^{11}g^{4-m}c_g^2} \quad, \tag{22}$$

where m is a tunable parameter. This scaling function represents a minor modification to the deep water scaling function of the DIA, modified to extend its applicability in intermediate water depths up to $kd \approx 0.75$. The shallow water scaling function represents a new result from this study, and is given as

$$B_{\text{shal}} = \frac{g^2 k^{11}}{(2\pi)^{11} c_g}(kd)^n, \tag{23}$$

where n is a tunable parameter, with typically $n = -3.5$.

2.5. Putting it all together

In the previous sections, all elements necessary to construct a shallow-water GMD from Eq. (7) are provided. Table 1 presents a general three-parameter quadruplet definition that can be reduced to the one-parameter quadruplet definition of the traditional DIA. These quadruplets need to be evaluated at the actual water depth (unlike in the traditional DIA) to assure conservation of energy, action and momentum. Combining Eqs. (7), (16), (18) and (21), the basic GMD equation corresponding to the DIA Eq. (9) becomes

$$\begin{pmatrix} \delta S_{nl,1} \\ \delta S_{nl,2} \\ \delta S_{nl,3} \\ \delta S_{nl,4} \end{pmatrix} = \begin{pmatrix} -1 \\ -1 \\ 1 \\ 1 \end{pmatrix} \left(\frac{1}{n_{q,d}} C_{\text{deep}} B_{\text{deep}} + \frac{1}{n_{q,s}} C_{\text{shal}} B_{\text{shal}} \right)$$
$$\times \left[\frac{c_{g,1} F_1}{k_1 \sigma_1} \frac{c_{g,2} F_2}{k_2 \sigma_2} \left(\frac{c_{g,3} F_3}{k_3 \sigma_3} + \frac{c_{g,4} F_4}{k_4 \sigma_4} \right) - \frac{c_{g,3} F_3}{k_3 \sigma_3} \frac{c_{g,4} F_4}{k_4 \sigma_4} \left(\frac{c_{g,1} F_1}{k_1 \sigma_1} + \frac{c_{g,2} F_2}{k_2 \sigma_2} \right) \right], \tag{24}$$

where the scaling functions B_{deep} and B_{shal}, representing weak and strong interactions, respectively, are given by Eqs. (22) and (23). Eq. (24) reduces to Eq. (9) when assuming deep water (and removing the shallow water scaling), and when using the original quadruplet definition (8). This equation for discrete source term contributions for individual discrete spectral grid points is applied to the entire spectrum as is done in the traditional DIA.

3. Numerical implementation

In most third-generation wave models source terms are integrated using a semi-implicit scheme, where the discrete spectral increment $\Delta F(f, \theta)$ is computed as (WAMDIG, 1988)

$$\Delta F(f, \theta) = \frac{S(f, \theta)\Delta t}{1 - \alpha \boldsymbol{D}(f, \theta)\Delta t}, \tag{25}$$

where $\alpha = 1$ determines the centricity of the scheme (Hargreaves and Annan, 2001). The term $\boldsymbol{D}$ represent diagonal contributions of the partial derivative of S_{nl} with respect to F and follows from Eqs. (24) and (20) as

$$\begin{pmatrix} \delta \boldsymbol{D}_1 \\ \delta \boldsymbol{D}_2 \\ \delta \boldsymbol{D}_3 \\ \delta \boldsymbol{D}_4 \end{pmatrix} = \begin{pmatrix} -P_1' \\ -P_2' \\ P_3' \\ P_4' \end{pmatrix} \left(\frac{1}{n_{q,d}} C_{\text{deep}} B_{\text{deep}} + \frac{1}{n_{q,s}} C_{\text{shal}} B_{\text{shal}} \right), \tag{26}$$

where

$$P_1' = \frac{c_{g,1}}{k_1 \sigma_1} \left[\frac{c_{g,2} F_2}{k_2 \sigma_2} \left(\frac{c_{g,3} F_3}{k_3 \sigma_3} + \frac{c_{g,4} F_4}{k_4 \sigma_4} \right) - \frac{c_{g,3} F_3}{k_3 \sigma_3} \frac{c_{g,4} F_4}{k_4 \sigma_4} \right], \tag{27}$$

$$P_2' = \frac{c_{g,2}}{k_2 \sigma_2} \left[\frac{c_{g,1} F_1}{k_1 \sigma_1} \left(\frac{c_{g,3} F_3}{k_3 \sigma_3} + \frac{c_{g,4} F_4}{k_4 \sigma_4} \right) - \frac{c_{g,3} F_3}{k_3 \sigma_3} \frac{c_{g,4} F_4}{k_4 \sigma_4} \right], \tag{28}$$

$$P_3' = \frac{c_{g,3}}{k_3 \sigma_3} \left[\frac{c_{g,1} F_1}{k_1 \sigma_1} \frac{c_{g,2} F_2}{k_2 \sigma_2} - \frac{c_{g,4} F_4}{k_4 \sigma_4} \left(\frac{c_{g,1} F_1}{k_1 \sigma_1} + \frac{c_{g,2} F_2}{k_2 \sigma_2} \right) \right], \tag{29}$$

$$P_4' = \frac{c_{g,4}}{k_4 \sigma_4} \left[\frac{c_{g,1} F_1}{k_1 \sigma_1} \frac{c_{g,2} F_2}{k_2 \sigma_2} - \frac{c_{g,3} F_3}{k_3 \sigma_3} \left(\frac{c_{g,1} F_1}{k_1 \sigma_1} + \frac{c_{g,2} F_2}{k_2 \sigma_2} \right) \right]. \tag{30}$$

This completes the equations needed for implementing the GMD in a wave model. Apart from this, numerical algorithms need to be optimized, particularly because the GMD is expected to dominate computational requirements of a typical wave model. Details of this optimization can be found in Section 5.1 of Tolman (2008b).

4. Parameter optimization

The GMD can be configured in many ways, with a potentially large number of free parameters. The optimization techniques used will be described here only cursorily. For a detailed description of the parameter optimization of the GMD reference is made to the companion paper (Tolman and Grumbine, 2013). The optimization uses three basic concepts; (i) holistic optimization, (ii) genetic optimization techniques, and (iii) incremental addition of complexity. These three main concepts are discussed in Section 4.1. Subsequently, deep and shallow water configurations and corresponding test results are presented in Sections 4.2 and 4.3, respectively.

4.1. Basic approaches

As mentioned in the introduction, it is essential to test interaction approximations using full model integration behavior, and not to fit the interactions for selected spectra only. A former approach appears to have been used by HHAB in a subjective manner for idealized wave growth conditions. Subsequent studies, however, generally consider fitting of interactions for test spectra only. The 'holistic' optimization approach using full model integration was re-introduced by Tolman and Krasnopolsky (2004) and Tolman (2005), introducing objective error measures not found in HHAB.

For the present study, six deep water and three shallow water tests were constructed, expanding upon the two deep water cases used in Tolman and Krasnopolsky (2004). The deep water tests consist of traditional duration- and fetch-limited growth cases, the 'homogeneous front' case of Tolman (1992), a one-point model with continuously turning winds, a slanting fetch case, and a case with wave growth in the presence of swell. The shallow water tests consist of a one-point model with wave growth in diminishing water depths, and both wind seas and swells approaching a beach. Numerical details on the implementation of the test cases can be found in Tolman (2010), Section 3.3.

For each test case approximately 50 spectra are saved. Results for each GMD configuration are compared to results obtained with the full nonlinear interactions according to the Webb–Resio–Tracy method (Webb, 1978; Tracy and Resio, 1982; Resio and Perrie, 1991), as implemented in WW3 using the portable software package of Van Vledder (2002a, 2006).[4] From the spectra obtained with the WRT and GMD approaches, errors for 15 wave parameters are computed, ranging from mean wave parameters such as significant wave height and peak wave frequency, to full two-dimensional spectra and nonlinear source terms.

A genetic optimization technique is used to simultaneously optimize many free parameters in the GMD. Details of the optimization procedures can be found in Tolman and Grumbine (2013).

Finally, GMDs with increasing complexity have been considered. First, deep water is considered only, then shallow water is added. First, a traditional DIA is considered with a one-parameter

---

[4] Model version 5.04 used here.

Table 2
Selected deep water GMD configurations with increasing complexity and accuracy. The WAM and WW3 configurations provide reference to present optional wave models. Note that settings of C_{shal}, m and n are irrelevant for the deep water test cases, and that $C_{shal} \equiv 0$ corresponds to a deep-water-only quadruplet. Model errors for idealized deep water test cases from Tolman and Grumbine (2013).

ID	λ	μ	θ_{12} (°)	C_{deep}	error (%)
WW3	0.250	–	–	1.00×10^7	25.1
WAM	0.250	–	–	3.00×10^7	26.5
G11d	0.231	–	–	2.54×10^7	21.2
G13d	0.126	–	–	5.80×10^7	15.7
	0.237	–	–	4.32×10^7	
	0.319	–	–	1.43×10^7	
G25d[a]	0.068	0.015	–	6.39×10^7	11.0
	0.115	0.077	–	3.58×10^8	10.9[b]
	0.192	0.125	–	4.35×10^7	
	0.248	0.066	–	3.23×10^7	
	0.349	0.145	–	1.87×10^7	
G35d	0.066	0.018	21.4	1.70×10^8	9.3
	0.127	0.069	19.6	1.27×10^8	
	0.228	0.065	2.0	4.43×10^7	
	0.295	0.196	40.5	2.10×10^7	
	0.369	0.226	11.5	1.18×10^7	

[a] Dropped as preferred configuration.
[b] Error with smoother added to model.

quadruplet definition, adding additional quadruplets, then the two and three-parameter quadruplet definitions are considered similarly.

4.2. Deep water

Following the argument of the previous paragraph, it is natural to first address the GMD in a traditional DIA configuration, that is, with one quadruplet and a one-parameter quadruplet definition. The resulting configuration is presented in Table 2 as the G11d configuration. For comparison with previous configurations, the table also presents the original DIA configuration as used in many wave models. This configuration is identified here as the WAM configuration, after the first model to use this configuration (WAM-DIG, 1988).[5] The Table also presents the default configuration in the WW3 model, identified as WW3. Finally, the Table shows the objective model errors as defined in Tolman and Grumbine (2013).

The next step in the optimization is to add more representative quadruplets of the traditional DIA type. Incrementally increasing the number of quadruplets while optimizing both λ and C_{deep} shows clear improvements for $n_q = 2$ or 3 quadruplets, but no notable additional improvements beyond $n_q = 4$ or 5 quadruplets, consistent with Hashimoto and Kawaguchi (2001) and Van Vledder (2005). The one-parameter quadruplet configuration allows for another optimization experiment where the spectral space is sampled with a (relatively large) number of pre-set values of λ, and where the corresponding interaction strengths C_{deep} are optimized individually. Such experiments independently confirm the saturation of improvements found above. A good balance between accuracy and economy (small n_q) appears to be found with $n_q = 3$. A corresponding configuration[6] is added to Table 2 as configuration G13d.

The next level of complexity to be introduced in the GMD are the two- and three-parameter quadruplet definitions. Optimiza-

tion has been performed by increasing the number of quadruplets from $n_q = 3$ to 6. A good balance between accuracy and costs appears to be found for $n_q = 5$. Corresponding GMD configurations[6] are presented in Table 2, which also shows a clear gain in model accuracy through the objective model error.

So far, the GMD configurations are selected looking at overall model errors only, without addressing actual model behavior. Below, a representative selection of results of the optimization tests is presented. Independent testing in realistic conditions will be presented in Section 5.

Fig. 1 presents the significant wave height (H_s), peak frequency (f_p), mean direction ($\overline{\theta}$), and directional spread (σ_θ) as a function of the offshore distance x for a slanting fetch case with offshore winds under a 45° angle with a straight coastline. Presented are the results for the six configurations defined in Table 2, as well as the reference model results obtained with the WRT approach to the nonlinear interactions (i.e., the model to be reproduced by the GMD).

The DIA-equivalent GMD configurations (WW3, WAM, G11d, red lines in Fig. 1) show clear errors in mean wave parameters compared to the reference solution (WRT, green lines). Wave height and peak frequency errors depend on the actual configuration. The mean direction ($\overline{\theta}$) is too close to the wind direction, and directional spread (σ_θ) is overestimated for all DIA equivalent configurations. The more complex GMD configurations (G13d, G25d, G35d, blue lines) generally show accurate representation of most mean wave parameters, with the exception of the G25d configuration (dashed blue line) resulting in clear errors for the mean wave direction ($\overline{\theta}$).

Fig. 2 shows some selected one-dimensional spectral results from the slanting fetch case at 30 km offshore. For the energy spectrum $F(f)$ (Fig. 2(a)), the DIA-equivalent models (red lines) underestimate the expected spectral peak energy (WRT, green line) by up to 40%. Increasing the complexity by going from the G13d configuration to the G25d and G35d configurations (blue lines) systematically reduces the differences with the reference solution (green line), with the latter two configurations removing most of the model error. The corresponding steepness spectra $G(f) = k^2 F(f)$ (Fig. 2(b)) highlight the behavior at higher frequen-

---

[5] Note that this represents the default WW3 model with the WAM configuration for the DIA, but not the default WAM model.
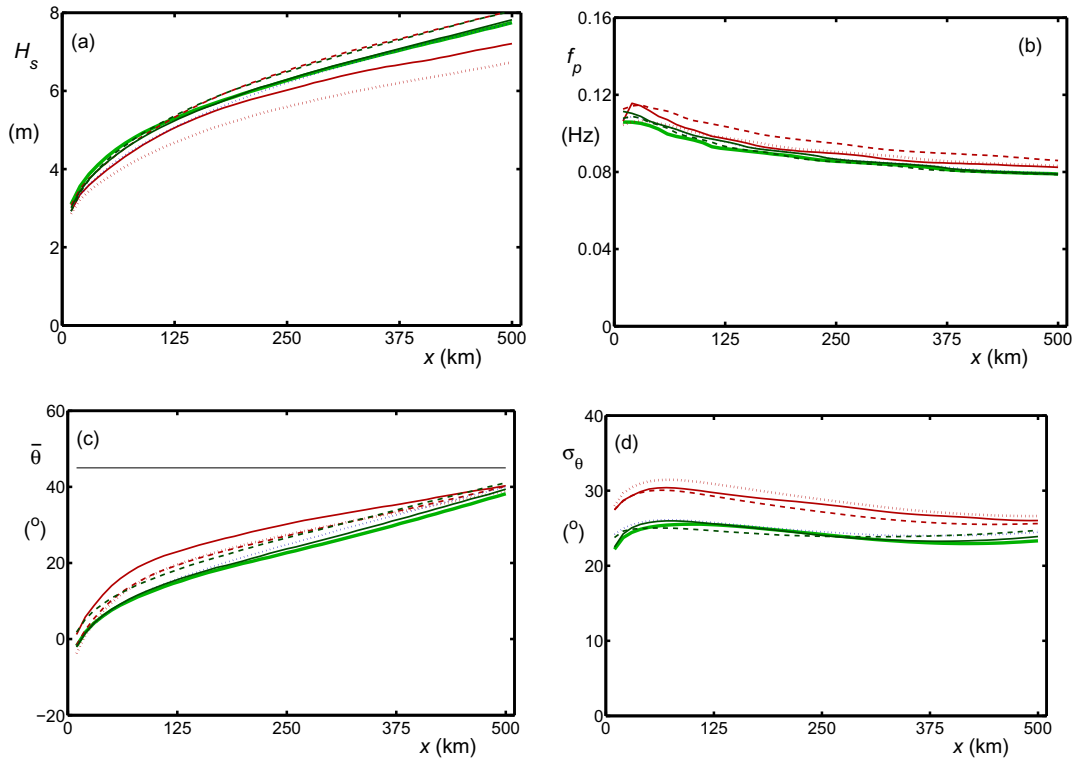[6] Tolman and Grumbine (2013) indicate that multiple near-optimum solution can be found.

Fig. 1. Evolution in space of (a) significant wave height H_s, (b) peak frequency f_p, (c) mean direction $\overline{\theta}$, and (d) directional spread σ_θ for a slanting fetch test with a wind under 45° with the coast. Green line: WRT. Dotted/dashed/solid red line: WAM/WW3/G11d. Dotted/dashed/solid blue lines: G13d/G25d/G35d. Solid black line in panel (c) represents wind direction.

cies, showing similar behavior as observed for the energy spectrum.

Fig. 2(c) shows the mean wave direction as a function of the wave frequency $\overline{\theta}(f)$, where 90° represents the direction perpendicular to the shore. At high frequencies, wave components line up with the wind direction where $\overline{\theta}(f) = 45°$. For lower frequencies, waves propagate more parallel to the coast with wave components with a period of approximately 10 s ($f \approx 0.1$ Hz) traveling parallel to the coast with $\overline{\theta}(0.1) \approx 0°$. At this offshore distance, longer wave components propagate toward the coast ($\overline{\theta}(f) < 0°$). The traditional DIA configurations (red lines) generally result in wave components that are lined up too much with the wind direction. The more advanced GMD configurations (blue lines) show a generally good representation of the reference model results (green line). Fig. 2(d) shows the directional spread as a function of the frequency $\sigma_\theta(f)$. As with the mean directional spread, the DIA-equivalent configurations overestimate spreads. Finally, Fig. 2(e) shows the nonlinear interactions as a function of the frequency $S_{nl}(f)$. All configurations show similar behavior, with only moderate improvements for more complex configurations.

Fig. 3 shows the corresponding energy and steepness spectra for the duration-limited growth test after 6 h of model integration. This test produces more typical spectra with strong peak enhancement and an equilibrium range with constant steepness above the spectral peak frequencies. In spite of the big differences in spectral shape compared to those of the slanting fetch case in Fig. 2, the relative behavior of the different GMD configurations is nearly identical, and the results for the WRT and G35d approaches are nearly identical.

Fig. 4 shows some two-dimensional wave spectra from the fetch-limited test case 30 km offshore. Whereas all spectra look similar due to the logarithmic scaling, there are nevertheless significant differences in the spectral shape between the reference

(WRT) model results and the DIA-equivalent (WAM) approaches. The G13d configuration removes most of the errors in the spectral shape but underestimates the peak energies, whereas the results of the G35d configurations follow the reference results most closely.

Fig. 5 shows the corresponding two-dimensional source terms. Although there are clear differences in details of the interactions, the distribution and magnitude of the interactions are surprisingly similar. This is in stark contrast with previous studies where different interaction approaches show large differences for test spectra. Apparently, the holistic optimization of the interactions favors relatively small differences in spectral shape to accommodate very similar interactions and corresponding fluxes in the full wave model. In spite of the relatively small differences, the more complex interaction approaches result in clearly superior interaction behavior when compared to the exact (WRT) results.

Note that the G25d configuration requires the use of the conservative high-frequency filter of Tolman (2011) to suppress high-frequency spectral noise (see Figs. 5 and 6 of the latter paper). Because the G25d and G35d are equally expensive to run, and the G35d configuration is clearly superior, G25d should be considered as a non-preferred configuration in Table 2.

4.3. Shallow water

The next step is to optimize shallow water behavior of the GMD. A simple way to limit the configurations to be considered is to start from previously optimized deep water configurations, and expand these to optimize shallow water behavior too. If shallow water variables (C_{shal}, m, n) are added to existing deep water quadruplets, or if shallow water quadruplets ($C_{deep} \equiv 0$) are added, then deep water test cases do not need to be addressed again. Consequently, only the three shallow water test cases need to be used in the optimization. In Tolman (2010), Section 4 a large number of configura-
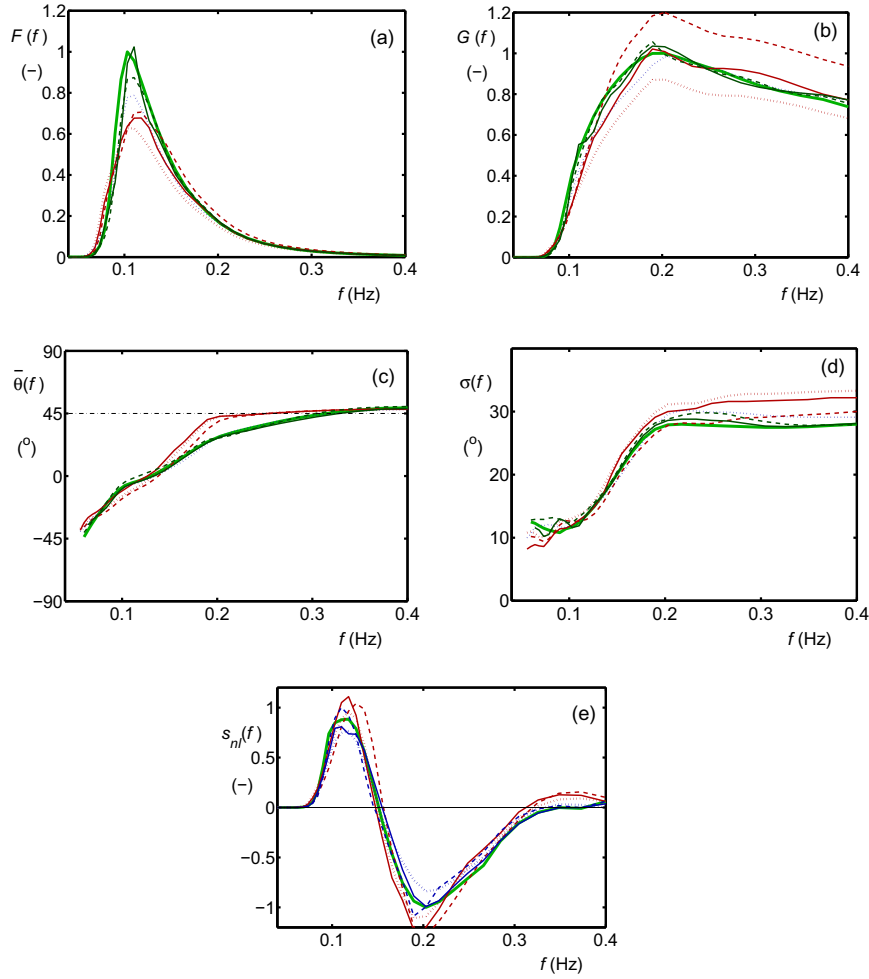
Fig. 2. One-dimensional spectral quantities at $x = 30$ km for slanting fetch case. (a) energy spectrum $F(f)$, (b) steepness spectrum $G(f)$, (c) mean direction $\overline{\theta}(f)$, (d) directional spread $\sigma_\theta(f)$. (e) Source term $S_{nl}(f)$. All variables normalized with the absolute maximum of the WRT results. Green line: WRT. Dotted/dashed/solid red line: WAM/WW3/G11d. Dotted/dashed/solid blue lines: G13d/G25d/G35d. Solid black line in panel (c) represents wind direction.
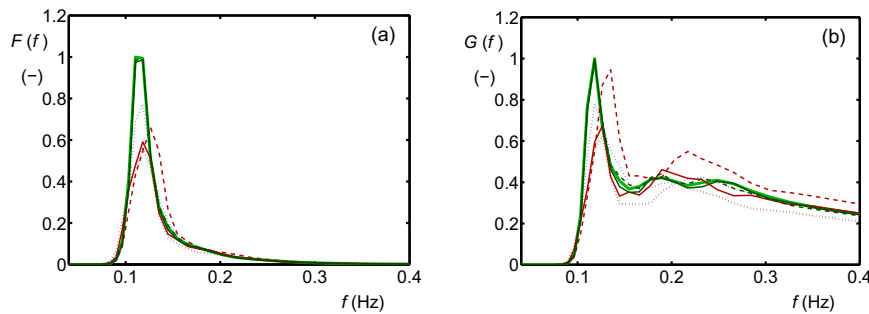
Fig. 3. Like Fig. 2 for duration-limited growth after 6 h of model integration, one-dimensional spectra only.

tions has been optimized. Here, only a few optimized configurations are presented in Table 3 to illustrate the potential and shortcomings of the GMD in representing strong four-wave interactions in extremely shallow water. Note that the deep-water scaling with $m = 0$ or m optimized separately, yields a GMD that is valid up to water depths as shallow as $kd \approx 0.75$. For more details on this optimization for intermediate water depths reference is made to Section 4 of Tolman (2010).

The G111 configuration consists of the traditional DIA configuration optimized for deep water, with a second fully optimized one-parameter shallow water quadruplet added. The G1ss config-

uration consists of 13 one-parameter quadruplets with pre-set values of λ. The deep water scaling functions use C_{deep} as previously optimized for deep water, whereas C_{shal} is optimized for each quadruplet. Note that one resulting quadruplet uses both deep and shallow water scaling, whereas four quadruplets are switched off using neither deep nor shallow water scaling. The G355 configuration uses the three-parameter quadruplet definition. It starts from the G35d configuration adding five quadruplets with shallow water scaling only. Note that three of the shallow water configurations effectively degenerate to the one-parameter quadruplet definitions with μ undefined or $\mu \approx 0$ and $\theta_{12} \approx 0$.
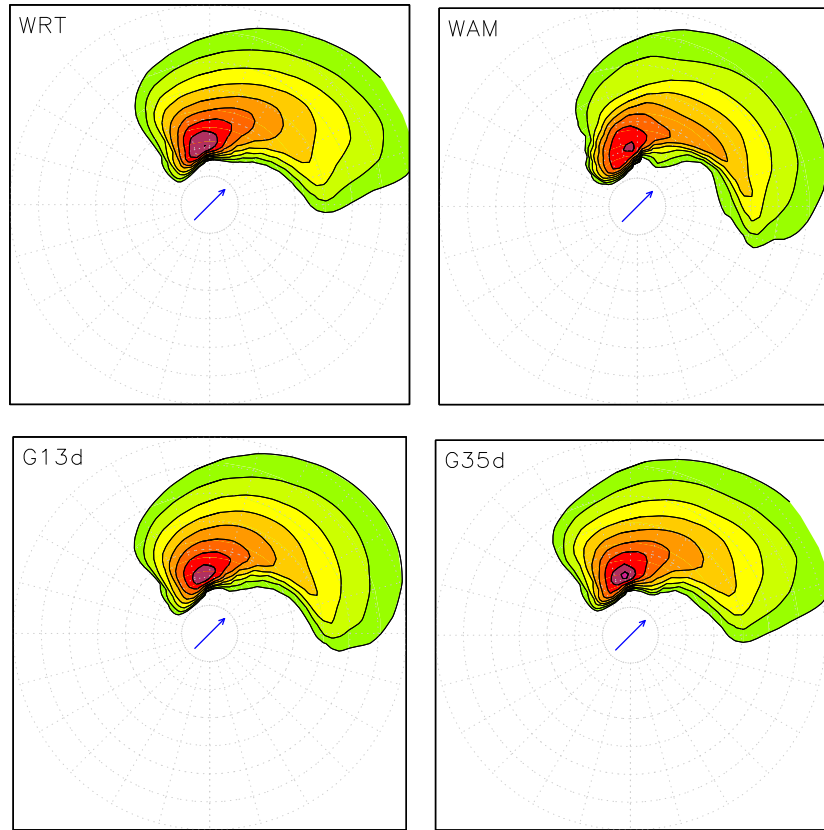
Fig. 4. Two-dimensional energy spectra $F(f, \theta)$ from approaches as indicated in the panels for the slanting fetch growth test 30 km offshore (third offshore grid point). Logarithmic scaling with factor 2 between contours and lowest contour at 0.10 m^2 s. Frequencies ranging from 0 to 0.25 Hz, frequency grid lines at 0.05 Hz intervals.

The representation of strong interactions in the GMD is most clearly illustrated in the test case with swell with $f_p = 0.07$ Hz breaking on a beach with a slope of 1:250. Resulting one-dimensional spectra and source terms for water depths of 3 and 1 m are presented in Figs. 6 and 7, respectively.

If the nonlinear interactions are switched off (red lines in figures), the spectra are transformed only due to shoaling and refraction. However, wave energy is not redistributed in frequency space, and hence the swell retains a sharp spectral signature as provided on the input boundary of the model. Results for the DIA, which does not represent strong interactions, are for all practical purposes identical to those without considering nonlinear interactions at all.

However, in extremely shallow water the strong interactions are capable of redistributing energy in frequency space (e.g., Janssen and Onorato, 2007). This is observed in Figs. 6 and 7 as the model with the WRT approach (green lines) results in clear interactions, as well as a clear spreading of the wave energy in frequency space. The various GMD configurations (G111, G1ss, G355) show a reasonable representation of the change in spectral shape, albeit with a spurious shift of energy to lower frequencies. Fig. 6(b) indicates that at 3 m water depth this spurious shift of energy is associated with a strong spurious signature in the nonlinear source term. In shallower water the impact of the interactions as well as the spurious shift of energy to lower frequencies in the GMD configurations becomes stronger, as is illustrated in Fig. 7 for a water depth of 1 m.

Spurious shifting of energy to low frequencies can have a large impact on coastal processes. Furthermore, the effects of four-wave interactions in extremely shallow water also needs to be addressed in the context of triad interactions (e.g., WISE Group, 2007), which are likely to be dominant in practical spectral transformations in the surf zone. As these interactions are neglected here, the results for the surf zone are not expected to be very realistic. Whereas the GMD results for extremely shallow water are clearly promising, this part of the GMD does not appear ready for operational wave modeling. Hence, only deep water scaling will be considered in the practical tests in the following section.

5. Practical application

So far, all test cases considered have also been used in the optimization, and are therefore not independent tests. Furthermore, the test cases are highly idealized. Whereas all test cases deal with model behavior necessary for practical models, they do not result in realistically complex wave conditions. Finally, tests in realistic conditions should be used to address computational costs of a wave model based on the GMD compared to models using the traditional DIA or the WRT approach.

One such test is an idealized hurricane modeled with three nested and moving grids (Tolman and Alves, 2005; Tolman, 2008a). The maximum wind speed is 45 m s^{-1}, and the radius of maximum winds is 50 km. The hurricane moves to the right (east) with a speed of 5 m s^{-1}. At the end of 24 h of model integration spectra at 33 output locations are saved.

Table 4 shows errors and normalized run times for various GMD configurations for the test. The errors for the traditional WAM and WW3 configurations are similar to those obtained with the idealized test cases (compare to Table 2). Furthermore, increasing complexity in the GMD configuration leads to a systematic reduction of errors, albeit with somewhat larger resulting errors than in the idealized test cases. Qualitatively, errors of the various GMD configurations are also similar to those of the idealized test cases, as will be illustrated below.
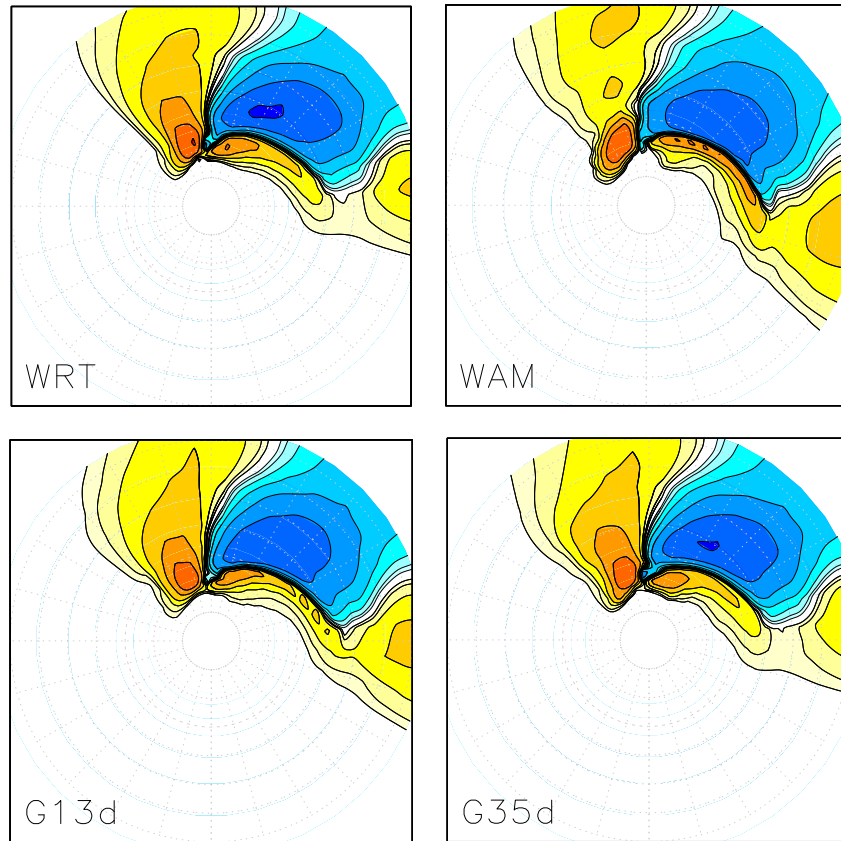
Fig. 5. Two-dimensional source terms $S_{nl}(f, \theta)$ corresponding to Fig. 4. Logarithmic scaling with factor 2 between contours and lowest contour at $\pm 1 \times 10^{-5}$ m^2. Blue colors identify negative values.
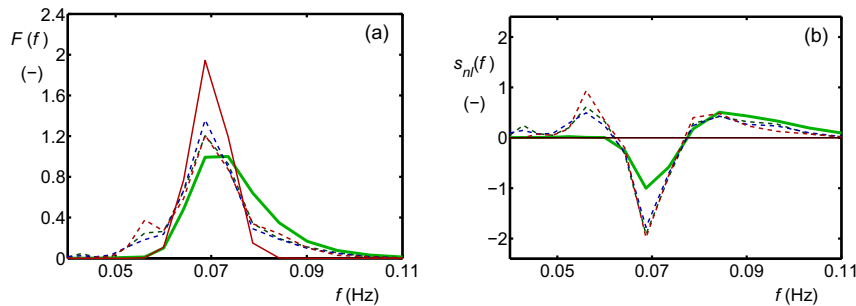

Fig. 6. Frequency spectra $F(f)$ (a) and one-dimensional source terms $S_{nl}(f)$ for the swell on a beach at 3 m water depth. Green line: WRT. Dashed green line: G355. Dashed blue line: G1ss. Dashed red line: G111. Solid red line: no interactions or DIA. Results normalized with maximum absolute value for WRT results.

Fig. 8a shows wave heights after 24 h of wave model integration from the hurricane test. The highest wave heights occur in the right front (southeast) quadrant of the hurricane, and exceed 12 m. Wave height errors in percent for the G11d, G13d and G35d configurations are presented in Figs. 8(b)–(d). For the traditional DIA configuration (G11d, Fig. 8(b)) systematic errors occur in most quadrants of the hurricane, with errors typically as large as 20%. Whereas error patterns for other DIA configurations such as WW3 and WAM are different, their magnitudes are similar (figures not presented here). For the G13d configuration (Fig. 8(c)), errors are greatly reduced with maximum errors generally below 10%, but spread over large areas. For the G35d configuration (Fig. 8(d)), wave height errors generally drop below 5%, and are localized rather than wide spread.

The hurricane test includes a wide range of spectra, including pure wind seas, pure swells, highly directionally sheared spectra,

and (transition to) multi-modal seas. Generally, the various GMD configurations behave as in the optimization tests, even for bimodal seas. This is illustrated in Fig. 9 with the model results for a location 100 km to the left (west) of the eye. At this location, a swell travels from the northern sector of the hurricane to the west, and a locally generated wind sea travels to the south (Fig. 9(a)). This results in a clearly bimodal energy spectrum $F(f)$ and steepness spectrum $G(f)$ (Fig. 9(b) and (c)), and a non-traditional signature of the nonlinear interactions (Fig. 9(f)). For all parameters presented in Fig. 9, increased complexity in the GMD results in improved model behavior, including an accurate description of the nonlinear interactions by the G35d configuration, where both spectral peaks contribute significantly to the interactions.

Finally, Table 4 shows normalized run times of the model using the selected GMD configurations. Run times are normalized with run times obtained with the default WW3 model settings (i.e.

Table 3
Selected GMD configurations for shallow water starting from configurations optimized for deep water. $n = -3.5$ in all configurations.

ID	λ	μ	$\theta_{12}(^o)$	C_{deep}	C_{shal}	m
G111	0.231	–	–	2.54×10^7	–	0
	0.184	–	–	–	1.63×10^5	
G1ss	0.100	–	–	–	4.96×10^4	-7.41
	0.125	–	–	7.84×10^7	–	
	0.150	–	–	–	–	
	0.175	–	–	–	–	
	0.200	–	–	–	6.54×10^5	
	0.225	–	–	2.12×10^7	–	
	0.250	–	–	7.12×10^6	–	
	0.275	–	–	1.66×10^7	–	
	0.300	–	–	–	–	
	0.325	–	–	–	–	
	0.350	–	–	9.00×10^6	3.52×10^5	
	0.375	–	–	–	5.04×10^5	
	0.400	–	–	–	1.84×10^5	
G355	0.066	0.018	21.4	1.70×10^8	–	-7.58
	0.127	0.069	19.6	1.27×10^8	–	
	0.228	0.065	2.0	4.43×10^7	–	
	0.295	0.196	40.5	2.10×10^7	–	
	0.369	0.226	11.5	1.18×10^7	–	
	0.036	0.003	4.2	–	2.54×10^5	
	0.105	0.104	0.5	–	1.58×10^7	
	0.184	–	1.9	–	7.40×10^5	
	0.360	0.225	44.1	–	5.04×10^8	
	0.375	–	0.0	–	1.03×10^6	
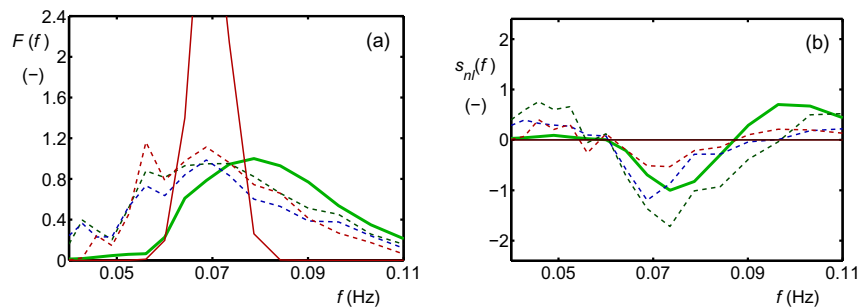
Fig. 7. Like Fig. 6 at 1 m water depth.

Table 4
Synopsis of model performance for hurricane test for various GMD configurations. T_n is the model run time, normalized with the results of the default wave model with the traditional DIA implementation.

ID	T_n (–)	Error (%)
WW3	1.20	27.5
WAM	0.99	28.7
G11d	1.05	26.3
G13d	1.50	19.1
G35d	3.53	14.9
WRT	1360[a]	–

[a] Estimated; additional resource needed to make model runs feasible.

using the original DIA implementation in the model). The GMD in WW3 configuration is equivalent to the default model, yet results in a model that is approximately 20% more expensive ($T_n \approx 1.2$) than the model using the traditional DIA implementation, due to the increased complexity of the GMD. The WW3, WAM and G11d configurations are all based on the traditional DIA configuration, and, therefore, require identical computational effort to compute a single interaction. Yet, the latter two configurations result in a more efficient model, with shorter normalized run times T_n. This appears to be associated with smoother model integration for the latter two configurations, resulting in an increase in the dynamically computed source term integration time step (see Tolman, 1992). The model configuration with three traditional quadruplets (G13d) results in a modest 50% increase in model run time ($T_n \approx 1.5$), whereas the most accurate GMD configuration (G35d) results in a more substantial increase of model run times by up to a factor of 3.5 ($T_n \approx 3.5$). However, the latter configuration removes most errors associated with the nonlinear interactions from the wave model, at a model cost that is more than two orders of magnitude less than the cost of using the full WRT interactions.

6. Discussion

The Discrete Interaction Approximation (DIA) has been the staple of third-generation wave models for decades. Whereas the authors of the DIA recognized some of its weaknesses, and numerous papers have been dedicated to improving or replacing the DIA (see Introduction), it is nevertheless still used in its original form in
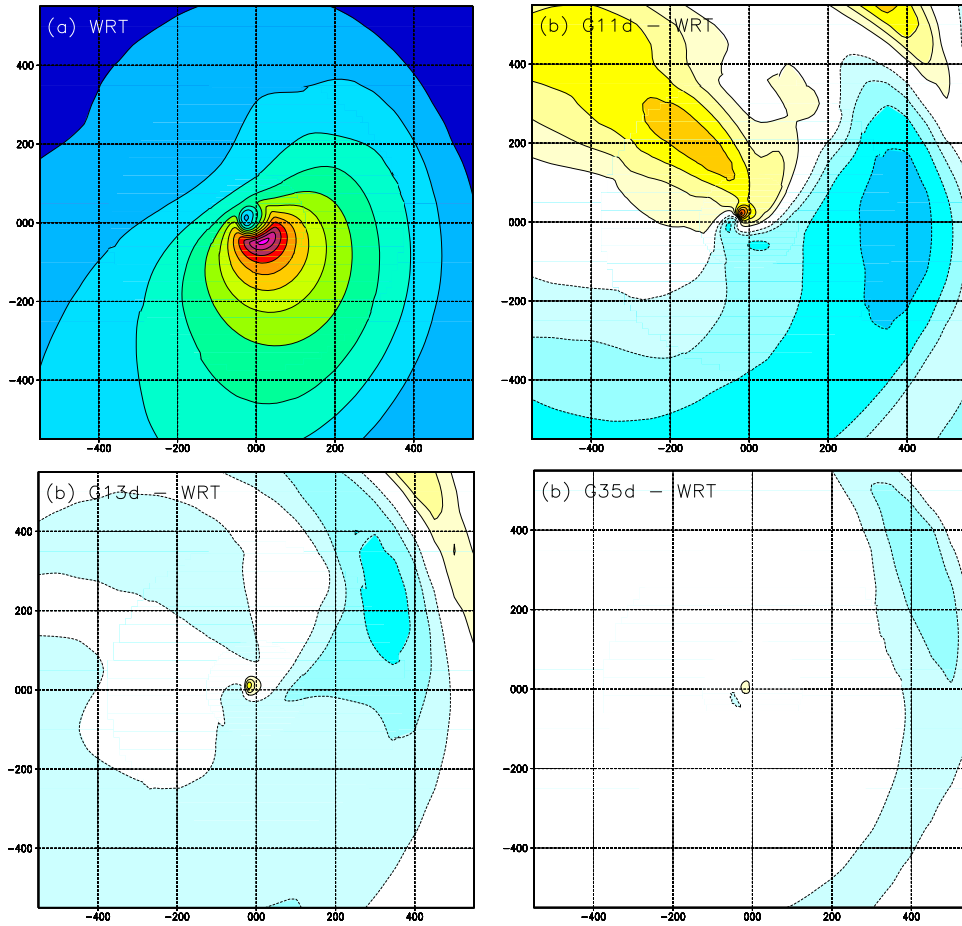
Fig. 8. Results of idealized hurricane test. (a) Significant wave heights of WRT computations at end of computation. Contours at 1 m interval, highest wave height over 12 m. (b)–(d) Wave height differences in % for various GMD configurations. Contours at 4% intervals, blue shading represent negative differences.
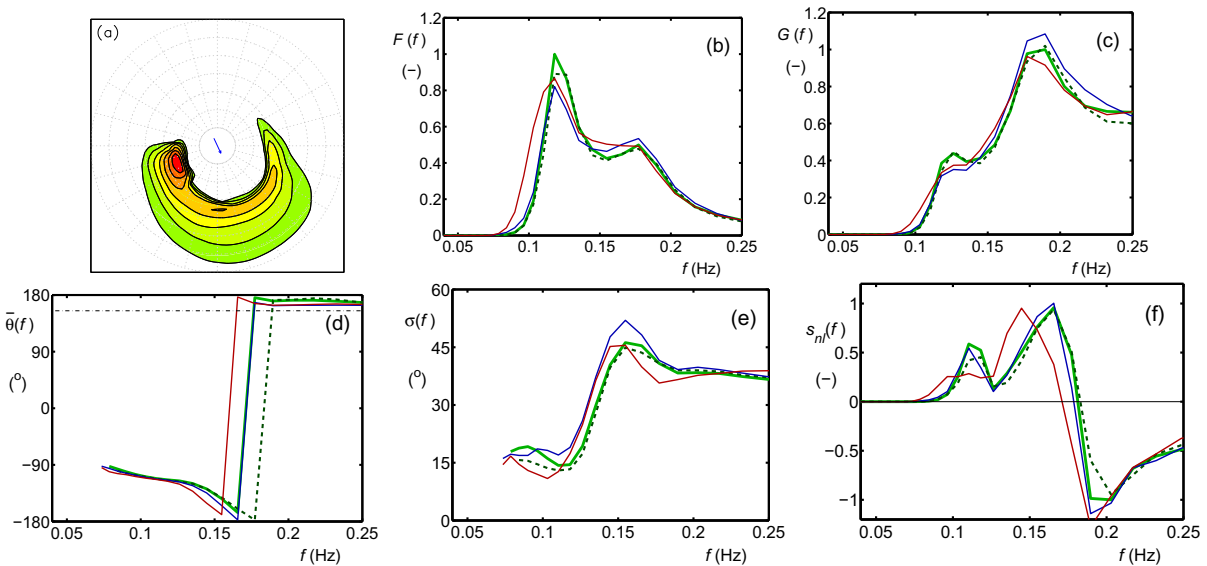

Fig. 9. Spectral behavior of various nonlinear approaches for output point 100 km left of eye of hurricane. (a) Two-dimensional spectrum $F(f, \theta)$, factor 2 increment in contour levels, lowest contour level at 10^{-4} m^2 s. (b) One-dimensional spectrum $F(f)$. (c) Steepness spectrum $G(f)$. (d) Spectral direction $\sigma_\theta(f)$. (e) Directional spread $\sigma(f)$. (f) Source term $s_{nl}(f)$. Green line: exact (WRT) solution. Dashed dark green line: G35d. Blue line: G13d. Red line: G11d.

most (operational) wind wave models. The present study presents an expanded version of the DIA, the Generalized Multiple DIA (GMD), which provides a more accurate alternative in deep water,

and expands the DIA to also represent strong interactions in extremely shallow water. In the following paragraphs various aspects of the GMD will be discussed.

The GMD utilizes an expanded quadruplet description. In addition to the traditional one-parameter quadruplet definition from the DIA, a two-parameter definition from Tolman (2004) and a new three-parameter quadruplet definition are available. The latter definition allows for arbitrary quadruplet configurations, and can be considered as a compact and symmetric form of a three-parameter definition of Van Vledder (2002b). The GMD uses the full limited-depth dispersion relation in all equations, including the depth-dependent configuration of quadruplets. The latter assures that the GMD conserves energy, action and momentum at arbitrary depths, unlike the DIA, which does not conserve momentum for limited water depths.

Traditionally the DIA is considered for intermediate to deep water conditions only, in which the nonlinear interactions are considered weak. In extremely shallow water, strong four-wave interactions occur (Webb, 1978), and the test cases used to optimize the GMD indicate that such interactions are strong enough to result in large changes in spectral shape. Whereas the GMD results in an adequate description of these interactions, it also results in some spurious shifting of energy to low frequencies. The latter behavior makes the GMD less suitable to represent strong interactions in shallow water. Two additional issues need to be considered with respect to the GMD in extremely shallow water. First, triad interactions are ignored in all computations performed here. Since these triad interactions are expected to dominate quadruplet interactions in extremely shallow water (e.g., WISE Group, 2007), GMD behavior in extremely shallow water may prove moot for operational wave models. Second, modification to the WRT computation method to expand their validity in shallow water as suggested by Janssen and Onorato (2007) are not yet included in the portable WRT package used here. Future GMD experiments with strong interactions in extremely shallow water need to be performed using these modifications.

Returning to weak interactions in intermediate and deep water, a traditional DIA configuration has been considered first. Using three traditional DIA quadruplets (G13d configuration in Table 2) removes most of the errors in the mean wave parameters, but leaves notable errors in spectral shapes and spectral parameters. Using five representative quadruplets with the full three-parameter quadruplet definition (G35d configuration) removes much of the remaining spectral errors. These errors for the dependent optimization test are confirmed by an independent realistic test case. The G13d configuration should be economically feasible in operational wave models, as it increases computational costs of the entire wave model by a modest 50%. The G35d configuration increases computational costs by a more substantial factor of 3.5. This may or may not be economically feasible in operational models, but it at least will result in near exact model behavior for research, with a model that is more than 2 orders of magnitude cheaper than one based on the exact WRT Boltzmann integration.

Several additional observations can be made from the results of the deep water idealized and realistic tests.

First, the conventional DIA configuration as used in the WW3 model results in a spectral peak that is systematically shifted to higher frequencies (see Fig. 3). This associates overestimation of spectral peak frequencies for wind seas with the default setting of this model. Note that the low-frequency part of the spectrum is described well, so that (initial arrival of) swell is expected to be described better than wind seas.

Second, it is well known that when different source term parameterizations like WRT or DIA are applied to the same spectrum, large differences are found in the resulting interactions. When the GMD is optimized to optimally represent full model integration behavior (holistic optimization), the opposite behavior occurs; interactions $S_{nl}(f)$ for different parameterizations and configurations are nearly identical (see Figs. 2(a) and (e), 4 and 5), at

the expense of notable differences in the shape of resulting spectra $F(f)$. Because the latter behavior is obtained by optimizing full model behavior, it appears that a good representation of nonlinear interactions (fluxes in the spectrum) is more important to describe the evolution of the wave field than an accurate description of details of the spectral shape. Whereas it is not intuitively clear why this should be the case, it does strongly support the need for holistic optimization of interactions rather than optimization of interactions for selected spectra.

Third, the realistic test case can give an indication of the magnitude of errors induced by the traditional DIA, as well as by various GMD configurations. Perhaps surprisingly, the DIA results in systematic errors of more that 20% in the wave height for hurricane conditions. A Lake Michigan test (see Tolman, 2010) shows smaller impacts on mean wave parameters, but similarly large impacts on spectral details.

The GMD configurations considered here are developed for the default configuration of the WW3 model version 3.14. There is no guarantee that the optimum GMD configurations found here are also suitable for other source term packages describing growth and decay of wind waves. At least, objective errors need to be recomputed for other physics packages. Possibly, the optimization experiments need to be repeated. Only if the configurations can be shown to be equally accurate for a range of physics packages, can the GMD configuration be considered as generally applicable.

7. Conclusions

A Generalized Multiple DIA (GMD) for nonlinear four-wave interactions in wind wave spectra is rigorously derived. The GMD expands on the traditional DIA by expanding the definitions of multiple representative quadruplets, formulating the expressions for arbitrary water depths, and by adding a scaling function to represent strong interactions in extremely shallow water (relative depths $kd \ll 0.5$). Optimization of free parameters of the GMD is performed by matching model behavior in test cases to model behavior obtained with the full Boltzmann integral description of the nonlinear interactions, and is presented in a companion paper (Tolman and Grumbine, 2013). In the present paper a cascade of deep and shallow water GMD configurations with increasing complexity and accuracy is presented. Results of the test cases used for the optimization of the free parameters in the GMD, and an independent test representing hurricane conditions show that the GMD is capable of removing most of the errors introduced by the DIA in deep water, at costs that are not prohibitive for operational wave modeling. Particularly in the hurricane test, errors introduced by the traditional DIA are surprisingly large, indicating the need for upgrading the nonlinear interaction parameterizations in operational wind wave models. In shallow water the GMD is capable of reproducing shallow water behavior of the exact interactions, albeit with some spurious shifting of energy to lower frequencies in extremely shallow water. The shallow water extension, therefore, does not seem ready for application in operational wave models, where its effects are most likely dominated by triad interactions anyhow.

References

Bretherthon, F.P., Garrett, C.J.R., 1968. Wave trains in inhomogeneous moving media. Proc. Roy. Soc. Lond. A 302, 529–554.

Gelci, R., Cazalé, H., Vassal, J., 1956. Ulitization des diagrammes de propagation à la prévision énergétique de la houle. Bulletin d'Information du Comité Central d'Océanographie et d'Études des Côtes 8, 169–197.

Gelci, R., Cazalé, H., Vassal, J., 1957. Prévision de la haule. La méthode des densités spectroangulaires. Bulletin d'Information du Comité Central d'Océanographie et d'Études des Côtes 9, 416–435.

Hargreaves, J.C., Annan, J.D., 2001. Comments on "Improvement of the short fetch behavior in the ocean wave model (WAM)". J. Atmos. Oceanic Technol. 18, 711–715.

Hashimoto, N., Kawaguchi, K., 2001. Extension and modification of discrete interaction approximation (DIA) for computing nonlinear energy transfer of gravity wave spectrum. In: Fourth International Symposium on Ocean Wave Measurement and Analysis. ASCE, pp. 530–539.

Hashimoto, N., Haagsma, I.G., Holthuijsen, L.H., 2002. Four-wave interactions in SWAN. In: Proc. 28th Int. Conf. Coastal Eng., ASCE, Cardiff, pp. 392–404.

Hasselmann, K., 1960. Grundgleichungen der seegangsvoraussage. Schiffstechnik 7, 191–195.

Hasselmann, K., 1962. On the non-linear energy transfer in a gravity wave spectrum. Part 1: General theory. J. Fluid Mech. 12, 481–500.

Hasselmann, K., 1963a. On the non-linear transfer in a gravity wave spectrum. Part 2: Conservation theory, wave-particle correspondence, irreversibility. J. Fluid Mech. 15, 273–281.

Hasselmann, K., 1963b. On the non-linear transfer in a gravity wave spectrum. Part 3: Evaluation of energy flux and sea-swell interactions for a Neuman spectrum. J. Fluid Mech. 15, 385–398.

Hasselmann, K., 1966. Feynman diagrams and interaction rules of wave-scattering processes. Rev. Geophys. Space Phys. 4, 1–32.

Hasselmann, S., Hasselmann, K., 1985. Computations and parameterizations of the nonlinear energy transfer in a gravity-wave spectrum. Part I: A new method for efficient computations of the exact nonlinear transfer integral. J. Phys. Oceanogr. 15, 1369–1377.

Hasselmann, K., Barnett, T.P., Bouws, E., Carlson, H., Cartwright, D.E., Enke, K., Ewing, J.A., Gienapp, H., Hasselmann, D.E., Kruseman, P., Meerburg, A., Müller, P., Olbers, D.J., Richter, K., Sell, W., Walden, H., 1973. Measurements of wind-wave growth and swell decay during the Joint North Sea Wave Project (JONSWAP). Ergänzungsh. Deutschen Hydrogr. Z., Reihe A 8 (12), 95 pp.

Hasselmann, S., Hasselmann, K., Allender, J.H., Barnett, T.P., 1985. Computations and parameterizations of the nonlinear energy transfer in a gravity-wave spectrum. Part II: Parameterizations of the nonlinear energy transfer for application in wave models. J. Phys. Oceanogr. 15, 1378–1391.

Herterich, K., Hasselmann, K., 1980. A similarity relation for the nonlinear energy transfer in a finite-depth gravity-wave spectrum. J. Fluid Mech. 97, 215–224.

Janssen, P.A.E.M., Onorato, M., 2007. The intermediate depth limit of the Zakharov equations and consequences for wave prediction. J. Phys. Oceanogr. 37, 2389–2400.

Komatsu, K., 1996. Development of a new generation wave forecast model based on a new schema of nonlinear energy transfer among wind waves (in Japanese). Ph.D. Thesis, Kyoto University, 155 pp.

Komatsu, K., Masuda, A., 1996. A new scheme of nonlinear energy transfer among wind waves: RIAM method – algorithm and performance. J. Oceanogr. 52, 509–537.

Komen, G.J., Cavaleri, L., Donelan, M., Hasselmann, K., Hasselmann, S., Janssen, P.A.E.M., 1994. Dynamics and Modelling of Ocean Waves. Cambridge University Press, 532 pp.

Masuda, A., 1980. Nonlinear energy transfer between wind waves. J. Phys. Oceanogr. 10, 2082–2093.

Phillips, O.M., 1960. On the dynamics of unsteady gravity waves of finite amplitude. J. Fluid Mech. 9, 193–217.

Phillips, O.M., 1981. Wave interaction: the evolution of an idea. J. Fluid Mech. 106, 215–227.

Rasmussen, J.H., 1998. Deterministic and stochastic modelling of surface gravity waves in finite depth. Ph.D. Thesis, Institute of Hydrodynamics and Water Resources (ISVA), Techn. Univ. Denmark.

Resio, D.T., Perrie, W., 1991. A numerical study of nonlinear energy fluxes due to wave–wave interactions. Part 1: Methodology and basic results. J. Fluid Mech. 223, 603–629.

Rice, S.O., 1944. Mathematical analysis of random noise. Bell Syst. Tech. J. 23, 282–332.

Snyder, R.L., Long, R.B., Neu, W.L., 1998. A fully nonlinear regional wave model for the Bight of Abaco 1. Nonlinear-transfer computation. J. Geophys. Res. 103, 3119–3141.

Sverdrup, H.U., Munk, W.H., 1947. Wind, sea and swell: theory and relations for forecasting. Tech. Rep. H.O. Pub. No. 601, United States Navy Department, Hydrographic Office.

SWAMP Group, 1985. Ocean Wave Modelling. Plenum Press, 256 pp.

Tamura, H., Waseda, T., Miyazawa, Y., Komatsu, K., 2008. Current-induced modulation of the ocean wave spectrum and the role of nonlinear energy transfer. J. Phys. Oceanogr. 38, 2662–2684.

Tolman, H.L., 1992. Effects of numerics on the physics in a third-generation wind-wave model. J. Phys. Oceanogr. 22, 1095–1111.

Tolman, H.L., 2003. Optimum discrete interaction approximations for wind waves. Part 1: Mapping using inverse modeling. Tech. Note 227, NOAA/NWS/NCEP/MMAB, 57 pp + Appendices.

Tolman, H.L., 2004. Inverse modeling of discrete interaction approximations for nonlinear interactions in wind waves. Ocean Modell. 6, 405–422.

Tolman, H.L., 2005. Optimum discrete interaction approximations for wind waves. Part 2: Convergence of model integration. Tech. Note 247, NOAA/NWS/NCEP/MMAB, 74 pp + Appendices.

Tolman, H.L., 2008a. A mosaic approach to wind wave modeling. Ocean Modell. 25, 35–47.

Tolman, H.L., 2008b. Optimum discrete interaction approximations for wind waves. Part 3: Generalized multiple DIAs. Tech. Note 269, NOAA/NWS/NCEP/MMAB, 117 pp.

Tolman, H.L., 2009a. Practical nonlinear interaction algorithms. In: 11th International Workshop on Wave Hindcasting and Forecasting & Coastal Hazards Symposium, JCOMM Tech. Rep. 52, WMO/TD-No. 1533, Paper J2.

Tolman, H.L., 2009b. User manual and system documentation of WAVEWATCH III ™version 3.14. Tech. Note 276, NOAA/NWS/NCEP/MMAB, 194 pp + Appendices.

Tolman, H.L., 2010. Optimum discrete interaction approximations for wind waves. Part 4: Parameter optimization. Tech. Note 288, NOAA/NWS/NCEP/MMAB, 175 pp.

Tolman, H.L., 2011. A conservative nonlinear filter for the high-frequency range of wind spectra. Ocean Modell. 39, 291–300.

Tolman, H.L., Alves, J.H.G.M., 2005. Numerical modeling of wind waves generated by tropical cyclones using moving grids. Ocean Modell. 9, 305–323.

Tolman, H.L., Grumbine, R.W., 2013. Holistic genetic optimization of a Generalized Multiple Discrete Interaction Approximation for wind waves. Ocean Modell. 70, 25–37.

Tolman, H.L., Krasnopolsky, V.M., 2004. Nonlinear interactions in practical wind wave models. In: Eighth International Workshop on Wave Hindcasting and Forecasting, JCOMM Tech. Rep. 29, WMO/TD-No. 1319, Paper E1.

Tracy, B., Resio, D.T., 1982. Theory and calculation of the nonlinear energy transfer between sea waves in deep water. WES Report 11, US Army Corps of Engineers.

Ueno, K., Ishizaka, M., 1997. On an efficient calculation method of the nonlinear energy transfer in wind waves. Sottukojiho JMA 64, 75–80 (in Japanese).

Van Vledder, G.P., 2000. Improved method for obtaining the integration space for the computation of nonlinear quadruplet wave–wave interaction. In: Proceedings of the Sixth International Workshop on Wave Forecasting and Hindcasting, pp. 418–431.

Van Vledder, G.P., 2001. Extension of the discrete interaction approximation for computing nonlinear quadruplet wave–wave interactions in operational wave prediction models. In: Fourth International Symposium on Ocean Wave Measurement and Analysis. ASCE, pp. 540–549.

Van Vledder, G.P., 2002a. A subroutine version of the Webb/Resio/Tracy method for the computation of nonlinear quadruplet interactions in a wind-wave spectrum. Report 151b, Alkyon, The Netherlands.

Van Vledder, G.P., 2002b. Improved parameterizations of nonlinear four wave interactions for application in operational wave prediction models. Report 151a, Alkyon, The Netherlands.

Van Vledder, G.P., 2005. The triplet method for the computation of nonlinear four-wave interactions in discrete spectral wave models. In: Edge, B.L., Hemsley, J.M. (Eds.), Fifth International Symposium on Ocean Wave Measurement and Analysis. ASCE (Paper 48).

Van Vledder, G.P., 2006. The WRT method for the computation of non-linear four wave interactions in discrete spectral wave models. Coastal Eng. 53, 223–242.

Van Vledder, G.P., Bottema, M., 2002. Improved modelling of nonlinear four-wave interactions in shallow water. In: Proc. 28th Int. Conf. Coastal Eng.. ASCE, Cardiff, Wales, pp. 459–471.

Van Vledder, G.P., Herbers, T.H.C., Jenssen, R.E., Resio, D.T., Tracy, B., 2000. Modelling of non-linear quadruplet wave–wave interactions in operational wave models. In: Proc. 27th Int. Conf. Coastal Eng.. ASCE, Sydney, Australia, pp. 797–811.

WAMDIG, 1988. The WAM model – a third generation ocean wave prediction model. J. Phys. Oceanogr. 18, 1775–1810.

Webb, D.J., 1978. Non-linear transfers between sea waves. Deep Sea Res. 25, 279–298.

WISE Group, 2007. Wave modelling – the state of the art. Prog. Oceanogr. 75, 603–674.

Young, I.R., Van Vledder, G.P., 1993. A review of the central role of nonlinear interactions in wind-wave evolution. Trans. Roy. Soc. Lond. 342, 505–524.

Zakharov, V.E., 1968. Stability of periodic waves of finite amplitude on the surface of a deep fluid. J. Appl. Mech. Tech. Phys. 2, 190–194.